HHS Public Access

Author manuscript

Magn Reson Imaging. Author manuscript; available in PMC 2016 December 01.

Published in final edited form as:

Magn Reson Imaging. 2015 December ; 33(10): 1224–1235. doi:10.1016/j.mri.2015.08.005.

A Non-Invasive Assessment of Cardiopulmonary Hemodynamics with MRI in Pulmonary Hypertension

Octavia Bane, PhD[1,2,3], **Sanjiv J. Shah, MD**[4], **Michael J. Cuttica, MD**[5], **Jeremy D. Collins, MD**[3], **Senthil Selvaraj, MD**[6], **Neil R. Chatterjee, BS**[2,3,6], **Christoph Guetter, PhD**[7], **James C. Carr, MD**[3], and **Timothy J. Carroll, PhD**[2,3]

[1]Translational and Molecular Imaging Institute, Icahn School of Medicine at Mount Sinai Hospital, New York, NY

[2]Biomedical Engineering, McCormick School of Engineering, Northwestern University, Evanston, IL

[3]Department of Radiology, Feinberg School of Medicine, Northwestern University, Chicago, IL

[4]Division of Cardiology, Feinberg School of Medicine, Northwestern University, Chicago, IL

[5]Division of Pulmonary and Critical Care, Feinberg School of Medicine, Northwestern University, Chicago, IL

[6]Feinberg School of Medicine, Northwestern University, Chicago, IL

[7]Siemens Corporation, Corporate Research, Princeton, NJ

Abstract

Purpose—We propose a method for non-invasive quantification of hemodynamic changes in the pulmonary arteries resulting from pulmonary hypertension (PH).

Methods—Using a two-element windkessel model, and input parameters derived from standard MRI evaluation of flow, cardiac function and valvular motion, we derive: pulmonary artery compliance (C), mean pulmonary artery pressure (mPAP), pulmonary vascular resistance (PVR), pulmonary capillary wedge pressure (PCWP), time-averaged intra-pulmonary pressure waveforms and pulmonary artery pressures (systolic (sPAP) and diastolic (dPAP)). MRI results were compared directly to reference standard values from right heart catheterization (RHC) obtained in a series of patients with suspected pulmonary hypertension (PH).

Results—In 7 patients with suspected PH undergoing RHC, MRI and echocardiography, there was no statistically significant difference ($p<0.05$) between parameters measured by MRI and RHC. Using standard clinical cutoffs to define PH (mPAP ≥ 25 mmHg), MRI was able to correctly identify all patients as having pulmonary hypertension, and to correctly distinguish

Send correspondence to: Timothy J. Carroll, 737 N Michigan Ave, Suite 1600, Chicago, IL 60611, t-carroll@northwestern.edu, Phone: 312-926-1733, Fax: 312-926-5991.

between pulmonary arterial (mPAP≥ 25 mmHg, PCWP<15 mmHg) and venous hypertension (mPAP ≥ 25 mmHg, PCWP ≥ 15 mmHg) in 5 of 7 cases.

Conclusions—We have developed a mathematical model capable of quantifying physiological parameters that reflect the severity of PH.

Keywords

pulmonary hypertension; two element windkessel; compliance; pulmonary vascular resistance

INTRODUCTION

Pulmonary hypertension (PH) is a disease of the pulmonary arteries that is characterized by increased pulmonary arterial pressure and vascular resistance. The pathophysiology of PH, with its two major subtypes, pulmonary arterial hypertension (PAH) and pulmonary venous hypertension (PVH), is complex: a variety of parameters reflecting change in flow, pressure, compliance and vascular pruning, which is reflected in the vascular resistance, are evaluated in patients suspected of having PH. While PVH is a consequence of left-sided diastolic dysfunction, PAH develops from physiological changes in the lung vasculature. The mechanism of PAH has been described [1,2] as an increase in vascular resistance and pressure due to the narrowing of the distal portions of the pulmonary arterial vasculature, which in turn leads to distension and loss of arterial compliance, C, in the proximal pulmonary arterial vasculature. The combination of increased pulmonary vascular resistance (PVR) and reduced arterial compliance increases the load on the right ventricle. If untreated, PAH leads to right ventricular failure and death.

Right heart catheterization (RHC) is the standard by which PH is differentially diagnosed and management of the disease is prescribed. PAH is defined clinically by a mean pulmonary artery pressure (mPAP) ≥25 mmHg at rest and pulmonary capillary wedge pressure (PCWP) ≤ 15 mmHg [3]. Elevated PCWP (> 15 mmHg) at RHC is used to distinguish PVH from PAH when mPAP≥ 25 mmHg [4]. PVR is also routinely calculated from RHC measurements, where a value greater than 3 Wood units (mmHg·min/L) reflects the increased resistance in PAH. From the pulmonary arterial pressure waveforms, systolic and diastolic values (sPAP and dPAP) are reported to characterize PH. sPAP (≥ 35–40 mmHg) is also used as a proxy for mPAP in the initial evaluation of PAH by Doppler echocardiography[4].

RHC is an invasive procedure with well-identified morbidity and mortality. While RHC is associated with a low rate of complications at experienced PH referral centers [5], the risk of complications, including death associated with RHC in sick PH patients may be higher at less experienced centers. Furthermore, the invasiveness of RHC makes periodic follow-up exams to assess therapeutic response or progression of the disease difficult. Therefore, a non-invasive, comprehensive, accurate assessment of cardiac function and pulmonary hemodynamics would be a major advance in the evaluation and management of patients with PH. We have developed a mathematical model, based on a non-contrast MRI exam, by which pathologic changes in pulmonary hemodynamics can be determined with a non-contrast MRI exam.

We show that information acquired in a non-contrast MRI exam can be used to derive parameters that are normally determined at cardiac catheterization. These parameters reflect the severity of PH and determine, among other things, the differential diagnosis between arterial and venous hypertension. When included in a windkessel model of pulmonary physiology, the parameters are able to quantify (in mmHg) intrapulmonary pressure waveforms non-invasively throughout then cardiac cycle. We describe the process by which C, PVR, PCWP, mPAP, sPAP, dPAP and the pressure-time waveform P(t) are determined in a 30 minute MRI exam. We have validated our approach against standard reference parameters measured by invasive RHC. The reliability of our method is assessed by intraclass correlation coefficients (ICC) for two independent observers.

MATERIALS AND METHODS

We evaluated our approach to hemodynamic quantification in a HIPAA compliant study which has been approved by the institutional review board (IRB). Patients with suspected PAH were recruited from the cardiology service at our institute prospectively and gave written, informed consent. The results of our MRI exams were analyzed and compared directly to standard of reference values of C, mPAP, PCWP, PVR, sPAP, dPAP and P(t) obtained by RHC. The MRI measurements of cardiopulmonary parameters were repeated by two independent observers, each with 5 years of experience in MRI post-processing, and verified by a board-certified cardiovascular radiologist with 10 years of experience. Echocardiograms were retrospectively included in our analysis to validate valve motion analysis, which yielded PCWP and PVR.

Patient Selection

Fourteen patients (12 females, 2 males, average age 55 years, age range 32–70 years) were recruited from February 2011 to December 2011. All patients were selected for inclusion by a board-certified cardiologist and met criteria for PH as defined by RHC (mPAP ≥ 25 mmHg) and subsequently underwent cardiac MR (CMR) imaging at 1.5T. As such, patients were pre-screened for any contra-indications to MRI (pacemaker, claustrophobia, BMI).

Of this patient cohort, six patients were excluded: four had uninterpretable RHC waveforms, one had no usable MR images of the pulmonary arteries, and one had an echocardiography exam more than a year before RHC. We validated our approach in a study of a sub-group of 8 patients (8 females, average age 56 years, age range 32–70 years). One patient was excluded from PVR analysis because an image series necessary for this analysis was not acquired. The remaining 7 subjects were included in the full analysis of all parameters (C, mPAP, PCWP, PVR, P(t)). The time interval between the RHC examination and MRI was one to ten days. The time between RHC and Doppler echocardiography varied between two weeks and two months, with no change in patient management in the time interval.

Echocardiography

All study participants underwent two-dimensional echocardiography with Doppler and tissue Doppler imaging. Echocardiography was performed using commercially available ultrasound systems with harmonic imaging (Philips iE33 or 7500, Philips Medical Systems,

Andover, MA; or Vivid 7, GE Healthcare, General Electric Corp., Waukesha, WI). Early mitral inflow (E) velocity and early diastolic tissue velocity (e′) were measured according to American Society of Echocardiography guidelines and PCWP was estimated non-invasively using the E/e′ ratio [6,7]. All echocardiographic measurements were made by a board-certified echocardiographer blinded to all other clinical data using ProSolv 4.0 echocardiographic analysis software (ProSolvCardioVascular; Indianapolis, IN).

Cardiac Catheterization

Right heart and pulmonary arterial (PA) catheterization was performed from either the right internal jugular or right femoral vein approach, at the discretion of the cardiologist performing the procedure, using standard Seldinger technique under fluoroscopic guidance. Participants underwent recording of invasive hemodynamics (mean right atrium pressure, sPAP, dPAP, mPAP and PCWP) using a fluid-filled, 6F PA catheter (Edwards Lifesciences, Irvine, CA) and a properly zeroed pressure transducer. Pressure recordings were analyzed off-line using a WITT Hemodynamic Workstation (Philips Medical Systems, Andover, MA) at a 50 mm/s paper speed with adjustment of pressure (mmHg) scale as needed. All hemodynamic pressure measurements were made at end-expiration and in duplicate using a standardized measurement protocol, by a trained investigator blinded to all clinical data. Cardiac output (CO) was calculated using the thermodilution method and PVR (Wood units) was calculated as:

$$\mathrm{PVR}=\frac{\mathrm{mPAP}-\mathrm{PCWP}}{\mathrm{RVCO}} \quad (1)$$

MRI

The right ventricle (RV) volume parameters for mPAP and the e′ for PVR were measured off standard ECG-gated steady state free precession cardiac CINE images (TrueFISP). The area and flow measurements for compliance and the velocity measurements for E were derived from standard MRI phase contrast pulse sequences. All MR imaging was performed on 1.5 T scanners (Magnetom Avanto, Espree, or Aera, Siemens Medical Systems, Erlangen, Germany). Post processing for the calculation of flow and ventricular function were performed on a standalone workstation (Argus, Siemens Medical Systems, Malvern, PA).

Cardiac function was defined based on TrueFISP CINE short axis images of the heart (FOV 300 mm × 380 mm, matrix size 109 × 192, TE 1.13 msec, TR 2.26 msec, BW 930 Hz, slice thickness 6 mm). Four chamber CINE images (FOV 300 mm × 350 mm, matrix size 192 × 256, TE 1.13 msec, TR 2.26 msec, slice thickness 6 mm) were acquired for measurement of the lateral mitral annular e′ velocity. For the compliance measurement, we measured cross-sectional area changes throughout the cardiac cycle using 2D phase-contrast flow images at the main, right, and left pulmonary arteries. Images were acquired during a 20 second breath-hold in a plane orthogonal to the pulmonary arteries (Figure 2), with FOV 300 mm × 350 mm, matrix size 100 × 192, TE 3.2 msec, TR 7.6 msec, slice thickness 6 mm, VENC=120 cm/s in the direction of the vessel.2D phase-contrast flow images (FOV 300 × 350 mm, matrix 128 × 128, TE 1.36 msec, TR 3.5 msec, VENC 80 or 120 cm/s, chosen to

maximize signal intensity while preventing aliasing) were acquired for the measurement of mitral inflow E velocity.

Data Analysis

We have developed a non-contrast image acquisition protocol and mathematical modeling that can quantify C, mPAP, sPAP, dPAP, PVR, PCWP, and intra-arterial pressure waveforms non-invasively. In the following section we describe the derivation of these parameters.

Pulmonary Artery Pressure Waveforms P(t)

Intra-pulmonary pressure waveforms contain additional information on the pressure change throughout the cardiac cycle. While time-resolved MRI flow waveforms in the pulmonaries are commonplace, non-invasive quantification of pressure waveforms has been elusive. The windkessel model [8] (Figure 1) is a well established mathematical model which relates pressure, compliance, vascular resistance, and blood flow. The two-element windkessel model has been established as a means of measuring ventricular after-load [8], particularly across short segments of the pulmonary arterial vasculature, where flow and pressure wave reflection is negligible [9]. In the following we use the windkessel model to derive a pressure versus time curve for the pulmonary arteries that incorporates the parameters derived above and addresses differences in systolic and diastolic flow through the inclusion/exclusion of a forcing function which describes the action of the right ventricle and mitral valve.

The two-element windkessel model allows expression of pulmonary pressure throughout the cardiac cycle, P(t), in terms of blood flow, Q(t), pulmonary arterial compliance, C, and pulmonary vascular resistance (PVR) as:

$$\mathrm{Q(t)}=\frac{P(t)}{PVR}+\mathrm{C}\frac{dP(t)}{dt} \quad (2)$$

Using linear time invariant system theory [10], the systolic pulmonary pressure waveform P(t) is modeled as the convolution of the input signal, pulmonary arterial flow with the system response, an exponential function (Equation 3, where $P(t_s)$ is the pressure at onset of systole, and Q(t) is the main pulmonary artery flow).

$$P_{systole}(\mathrm{t})=\frac{1}{C}\left(\mathrm{Q(t)}\otimes e^{-\frac{t}{PVR\,C}}\right)+\mathrm{P}\,(t_s)\,e^{-\frac{t}{PVR}} \quad (3)$$

During diastole, pulmonary pressure can be calculated as an exponential decay from end systolic pressure $P(t_{es})$, with the product of PVR and compliance as the decay constant, similar to the RC time constant of the parallel circuit shown in Figure 1.

$$P_{diastole}(\mathrm{t})=P(t_{es})e^{-\frac{t}{PVR\,C}} \quad (4)$$

In order to quantify pressure waveforms throughout the whole cardiac cycle using Equations 2–4, we need to determine PVR, C, $P(t_{es})$ and $P(t_s)$. The conditions that $P_{\text{end systole}} = P_{\text{beginning diastole}}$, as well as $P_{\text{end diastole}} = P_{\text{beginning systole}}$ from one cardiac cycle to the next, constrain the relative normalization of the two curves. Furthermore, the time-averaged pressure curve must be equal to the mean arterial pressure (mPAP). mPAP (mmHg), as well as PVR (mmHg min/L) and C (ml/mmHg) were determined non-invasively from non-contrast MRI exams as described above.

Validation of Two Element Windkessel Model

Initially, we validated our model of P(t) by convolving the MRI flow waveform in the main PA and the parameters PVR, C and mPAP measured by RHC in MatlabR2009a (Mathworks, Natick, MA). By setting the boundary condition that pressure at end systole equals the pressure at the beginning of diastole, the constants $P(t_{es})$ and $P(t_s)$ in Equations 3 and 4 were normalized to 1. The pressure curve was scaled by the mPAP from RHC.

P(t) derived from MRI parameters

The P(t) waveform was also calculated from the non-invasively derived MRI parameters and flow waveform. For comparison, it was also calculated from the MRI flow waveform, PVR and mPAP by MRI, and C measured by RHC.

Compliance (C)

Pathologic pressure increases in the pulmonary arteries result in vascular remodeling, which manifests itself as a loss in compliance. It has been shown that total pulmonary arterial compliance, C, of the pulmonary arterial tree can be estimated from the sum of proximal arterial volume compliances in the main, left and right pulmonary arteries [11]. There are a number of ways to measure compliance with MRI [2,8,11–21]. We determined area compliance from variables measurable by MRI alone using the following expression as proposed by Vulliemoz et al.[9]:

$$C_A = \frac{(\Delta A)^2 A}{(\Delta Q)^2 \rho} \quad (5)$$

where A is minimum (diastolic) area, ΔA change in vessel cross-section between systole and diastole, ΔQ change in flow between systole and diastole, and ρ density of blood.

The cross-sectional area, as well as flow, was measured in all three proximal pulmonary branches at peak systole (maximum area) and end diastole (minimum area), using vendor supplied post-processing software (Argus, Siemens Medical Solutions, Malvern, PA, USA). This process is described schematically in Figure 2. Volume compliance was obtained by multiplying local area compliances, C_A, by previously reported vessel lengths (2 cm in main PA, 3 cm in right, and 3 cm in left PA) [11] to obtain volume compliance (capacitance). Total lung vascular compliance (C) was estimated from the sum of proximal compliances using a previously reported approach [11].

Mean Pulmonary Arterial Pressure (mPAP)

From the reduced volumetric parameters of right ventricle (RV) function in pulmonary hypertension patients, mPAP can be estimated non-invasively based on pressure-volume loops. It has been shown in MR fluoroscopy cardiac catheterization exams that the RV end diastolic volume (EDV) and ejection fraction (EF) were statistically different in pulmonary hypertension patients, and were correlated with mPAP[22]. We use a similar approach to derive mPAP from the linear relationship between catheter-measured mPAP and the EDV/EF ratio measured from cardiac function images.

Pulmonary Capillary Wedge Pressure (PCWP)

The pulmonary capillary wedge pressure is a proxy measure of the left ventricle end diastolic pressure (LVEDP) in RHC. It is used to characterize the pressure load on the left ventricle, and thus to distinguish between arterial and venous hypertension. In clinical echocardiography practice, PCWP and LVEDP are often estimated from the ratio E/e′, where E is the peak early diastolic mitral inflow velocity and e′ is the peak early diastolic mitral annular velocity. The distribution of age-matched E/e′ values is used to characterize diastolic dysfunction [4,6]. In echocardiography, the E/e′ ratio is used as a predictor of PCWP through the linear relationship derived empirically by Nagueh et al [7]: $PCWP_{ECHO} = 1.24 * E/e' + 1.9$. In our analysis we have chosen the lateral e′, instead of septal e′, because basal septalmitral annular e′ tissue velocity reflects both RV and LV diastolic function. In addition, in patients with PAH, abnormal septal motion (septal flattening) due to RV overload is common. Thus, in patients with PAH, E/lateral e′ is a more accurate indicator of left atrial pressure. The equivalent parameterization for MRI is $PCWP_{MRI} = 0.77 *(E/e')_{MRI} + 1.9$.

Both E and e′ were measured by tissue Doppler echocardiography, the clinical standard, as well as by MRI. Mitral inflow velocity E was measured from 2D phase-contrast flow images by a commercial software package (Argus, Siemens Medical Solutions, Malvern, PA, USA). The septal and lateral wall e′ velocities were measured from high temporal resolution four chamber CINE images on a prototype software package (Cardiac UI, Siemens Corporate Research, Princeton, NJ) that automatically detects and tracks the mitral valve insertion points in the basal myocardium on four chamber TrueFISP CINE images [23]. MRI measurements were validated against those obtained at trans-thoracic Doppler echocardiography.

Pulmonary Vascular Resistance (PVR)

Pulmonary vascular resistance is a direct measure of the underlying conditions that precipitate PAH. Increased vascular resistance is the target of newer therapies that are intended to slow the progression of PAH. We calculate PVR through the simple relationship that is used in catheterization exams (Equation 1).

In cardiac catheterization, right ventricular cardiac output (RV CO) is determined via thermodilution. In MRI RV CO is determined from the systolic/diastolic ventricular volumes. The non-invasive derivation of mPAP and PCWP were described above.

sPAP/dPAP

Having quantified the pulmonary artery pressure waveform in three ways, the systolic and diastolic pressures can be read directly from the waveform. We report the maximum and the minimum points of the P(t) waveforms calculated in Matlab, up to 3 significant digits. The sPAP and dPAP values characterize the mean pressure, as well as the shape of the model-derived waveform compared to the RHC waveform.

Comparison with Three Element Windkessel

We sought to improve non-invasive quantification of PA pressure at MRI by applying the three element windkessel model through the addition of a characteristic impedance term estimated at MRI. Under the same assumptions of unidirectional and reflectionless waves, characteristic impedance can be expressed as $Z_c = (\rho/(A*C_A))^{1/2}$, as a function of the area compliances calculated as above. The calculation of diastolic pressure by the three element windkessel is identical to Equation 4; systolic pressure contains an additional Zc term, as in Equation 6.

$$P_{systole}(\mathrm{t}) = \frac{1}{C}\left(\mathrm{Q}(\mathrm{t}) \otimes e^{-\frac{t}{PVR\,C}}\right) + \mathrm{P}\,(t_s)\, e^{-\frac{t}{PVR}} + Z_c\, e^{-\frac{t}{PVR\,C}} \quad (6)$$

Statistical Analysis

We hypothesize that the values derived from cardiac MRI were in agreement with those derived from right heart catheterization (RHC). The mean values of C, mPAP, PCWP, PVR, sPAP, dPAP measured by MRI were compared to mean values derived from cardiac catheterization values using a paired Student's t-test with significance defined at the 5% level. The strength of correlation between echocardiography and MRI-derived E and lateral e′, as well as between MRI and RHC parameters, was determined by calculating Spearman correlation coefficients. We used the Spearman correlation because, although we test for linearity, we do not assume a linear relationship between the measurements.

Post-processing was performed in two instances 12 months apart by the first observer, and repeated by the second observer. We used the intraclass correlation coefficient (ICC) for two-way, random single measures to describe intraobserver and interobserver reliability [24].

RESULTS

All 7 patients who underwent analysis of all hemodynamic parameters (C, mPAP, PCWP, PVR, P(t), sPAP, dPAP) met invasive hemodynamic criteria for PAH (mPAP>/= 25 mmHg). Although all 7 patients were referred for RHC for suspected PAH, after invasive hemodynamic evaluation, 4/7 had PAH (PCWP </= 15 mmHg) whereas 3/7 had PVH (PCWP > 15 mmHg). All 7 patients had elevated PVR (> 2.5 Wood units). MR imaging, including the 20-second breath hold, was well tolerated by all patients. The comparison of MRI to RHC measurements of C, mPAP, PCWP, PVR, sPAP and dPAP for the 7 patients is

shown in Table 1. No statistically significant differences between MRI and catheterization values were observed.

Validation of Model

The sPAP and dPAP values obtained from our implementation of the two element windkessel model, with the MRI flow waveform and RHC cardiopulmonary parameters showed excellent correlation with the true sPAP (Spearman correlation 0.9286) and dPAP (Spearman correlation 1) measured from the RHC waveform (see Table 1). The model-derived sPAP value under-estimated true sPAP for patient 5 (sPAP RHC of 82 mmHg versus model sPAP of 68.4 mmHg). For this patient, the MPA flow waveform had the lowest temporal resolution (45 msec compared to 15–25 msec for the other patients), which explains the poor resolution of the systolic peak in the flow waveform and the resulting pressure waveform.

P(t), sPAP, dPAP from MRI parameters

The pressure waveforms calculated from MRI parameters showed agreement with those at RHC for patients with moderate PH (Figure 3). The sPAP and dPAP values measured of the pressure waveforms were not statistically different from their RHC counterparts (Table 1). sPAP values from MRI showed good correlation (0.61 Spearman correlation) with RHC, while the correlation for dPAP between MRI and RHC was poor (−0.04). Intraobserver agreement for dPAP and sPAP was good, as denoted by high ICC's of 0.81 and 0.9, respectively. However, the inter-rater agreement for dPAP and sPAP was modest (ICC=0.4) and poor (ICC=0.25), respectively.

P(t), sPAP, dPAP from flow, PVR and mPAP by MRI and C measured by RHC

Given the poor interobserver agreement in measuring compliance, we repeated the pressure waveform calculations with RHC compliance and all other parameters measured by MRI. The sPAP values show good Spearman correlation with true RHC sPAP (Spearman correlation of 0.78). dPAP values show poor Spearman correlation, due to scaling of the model pressure waveform by $mPAP^{MRI}$.

Pressure Wave Forms from the Three Element Windkessel Model

The addition of the impedance term to form a three element windkessel model resulted in less than 0.1% change in the pressure measured by MRI, even when the input impedance modulus was used as a proxy for characteristic impedance.

Compliance is within the expected range for patients at ≤ 2 ml/mmHg, versus 0.001–10 ml/mmHg in the normal population, with one exception, and values closely follow those obtained by the ratio of stroke volume over pulse pressure measured by RHC. The preliminary data from which compliance was calculated is summarized in Table 2. The Bland Altman plot of compliance (Figure 4) shows a mean difference of −0.23 ml/mmHg between the two methods. C exhibits good Spearman correlation between the two measurements (rho=0.89). Intraobserver reliability of compliance measurements was excellent (ICC=0.78), although interobserver reliability was poor (ICC <0.1)

mPAP RHC and RV EDV/EF in the 8 patients initially recruited for mPAP analysis display a linear relationship with slope 1.71 and intercept 31.84 (R^2=0.46) (Figure 5). The RV volume data, with its ICC's, is summarized in Table 3. Linear regression of true RHC mPAP on mPAP predicted from MRI using the linear RV EDV/EF dependence shows a linear relationship with slope 1.06 and intercept −2.3, and Spearman correlation of 0.82 (Table 1). The Bland Altman plot (Figure 6) shows almost null mean difference and a distribution of values within two standard deviations of the difference. Both intraobserver (ICC=0.97) and interobserver (ICC=0.93) ICC's showed excellent reproducibility of the mPAP measure (Table 1).

The E, e′ and PCWP values from which the PVR was calculated are summarized in Table 4. Good Spearman correlations (0.82 and 0.7, respectively) were obtained between E and e′ values measured by MRI and echo. A paired t-test showed that e′ is statistically different. We attribute this to the different methodology we follow for the measurement of e′, as outlined above. The parameterization we propose for the determination of PCWP compensates for the observed difference in the values. MRI PCWP under-estimates true RHC PCWP in 2 out of 7 cases, while echo PCWP differs by 40–50% from RHC PCWP in 3 out of 7 cases. The Bland Altman plot (Figure 6) shows agreement between PCWP MRI and PCWP RHC, with mean difference −1.67 mmHg. PCWP measurements by MRI showed excellent intraobserver and interobserver agreement, with ICC 0.99 and 0.97, respectively (Table 4). E and e′ measurements showed excellent intraobserver and interobserver agreement, with ICC values greater than 0.9.

PVR values were elevated for patients when compared to expected normal values (2–33 mmHg*min/L, vs <2 mmHg*min/L in the normal population). Linear regression of true RHC PVR on PVR predicted from MRI shows a linear dependence with slope 0.32 and intercept 2.9, Spearman correlation of 0.43 (Figure 4, Table 1). The Bland Altman plot shows a difference of 1.62 Wood units between RHC and MRI measurements (Figure 4). PVR measurements showed good intraobserver agreement (ICC=0.83), and acceptable interobserver reproducibility (ICC=0.69).

DISCUSSION

We have shown that it is feasible to quantify hemodynamic parameters that reflect pathologic changes resulting from pulmonary hypertension non-invasively by MRI. Hemodynamic values derived from MRI are in agreement with more invasive measurements based on RHC exams in patients with confirmed pulmonary hypertension. Furthermore, the MRI measurements exhibit high intra and inter-observer reproducibility. We derived many of the input parameters for the two element windkessel model from standard non-contrast cardiac MRI. Thus, our technique does not require the use of MR contrast agents, making it suitable in patients with renal co-morbidities who are poor candidates for gadolinium based MR angiography.

Compliance

Compliance has been correlated with mortality in PH patients [1], and in addition to mPAP and PVR it is being recognized as an important parameter for understanding PAH.

Compliance can be measured directly by RHC (stroke volume over pulse pressure, SV/PP), or indirectly by post-processing of catheter pressure-time waveforms and MRI flow waveforms, using a two- or three-element windkessel model. Direct estimation of compliance from catheter pressure and MRI flow and/or area measurements has also been used.

In this paper, we use a method to compute total vascular compliance, C, from local area compliance. Local area compliance, the ratio of change in lumen area and change in pressure between systole and diastole, can be estimated from MR images by a method previously used to measure compliance in the aorta [9]. The local area compliance measurement depends on the size of the main three PA branches, which has been previously shown to correlate with vasoreactivity and mPAP in PH patients of different etiologies [21,25]. However, our volume compliances are higher than those measured by methods using a combination of RHC and MRI. Although our compliance values over-estimate compliance measured by these methods, the values are in agreement with the non-invasive method used by Reuben to derive pulmonary arterial C from arterial transit time measured by N_2O plethysmography [17]. For further comparison, arterial transit time can be measured non-invasively by contrast enhanced MRA [26] and used in the same way to estimate mPAP, C and PVR.

Intra- and inter-rater agreement for compliance was low in our study. This is somewhat expected given the mathematical expression for compliance (Equation 5), in which even slight variability in flow measurements is amplified by squaring and inverting the flow difference. The ICC's calculated for all the parameters used to obtain compliance show that there is excellent agreement (ICC>90) within and between observers when measuring maximum and minimum area, and maximum flow. However, the agreement in measuring minimum flow is poor. Since signal intensity in phase contrast MRI is flow dependent, vascular boundaries are difficult to distinguish in the frames of low flow. Thus, there is great variability among raters in choosing the frame with minimum flow, and in contouring the arterial cross-section in the image with low flow. This shortcoming of our technique can be addressed by measuring vessel cross-section area by imaging techniques such as TrueFISP [27], combined with automatic edge-detection and motion coregistration [27] post-processing.

E and e′ velocities

A similar study in a small number of healthy volunteers reported substantial concordance correlations (0.6) between MRI and Doppler echocardiography measurements of E velocity and the combined lateral and septal e′ velocity [23]. In our study, we used lateral wall e′ instead of a combined septal and lateral e′ measurement, because of septal wall flattening due to RV overload in PAH patients.

mPAP, PCWP and PVR—We estimated mPAP by MRI from the linear relationship between mPAP by RHC and the RV EF/EDV ratio. The strong correlation with RV volumetric parameters is consistent with published findings showing shifts in the RV pressure-volume loops of PH patients [22]. Swift et al. have shown the empirical

dependence of mPAP on MRI parameters that reflect ventricular remodeling in pulmonary hypertension, namely interventricular septal angle and the ratio of RV/LV myocardial mass derived from ventricular volumes [28].

The same investigators identified left atrium (LA) size adjusted for body surface area as a physiological predictor of PCWP, with moderate correlation (Pearson's rho 0.58–0.7) between MRI-derived and RHC PCWP [28]. We obtained a similar correlation value (Pearson's rho 0.54) for PCWP derived from invasive and non-invasive method. A limitation of relating PCWP to MRI markers of LV filling pressures is that PCWP is itself a surrogate, not a direct measurement, of LV end-diastolic pressure. Correlations between MRI markers of LV filling pressure and a direct left-heart catheterization measurement of LV end-diastolic pressure are expected to be stronger [28].

PVR was calculated in our study and by other investigators [28] from MRI-derived mPAP, PCWP and RV CO. Alternatively, Garcia et al. estimated PVR from MPA flow and EF measured by cardiac MRI by a multivariate statistical model [29]. For PVR, we obtained a modest correlation (Pearson's rho=0.43) between the RHC and MRI-derived value compared to other studies with a large number of patients (Pearson's rho =0.8) [28,29].

Pressure values and waveforms

The dPAP and mPAP values computed from the two-element windkessel model show greement with RHC values. However, in patients with moderately to greatly elevated mPAP (> 30 mmHg), the sPAP is underestimated, while in borderline PH patients with low mPAP (~25 mmHg), sPAP, dPAP and mPAP are over-estimated. This is due to scaling of the pressure waveforms by $mPAP^{MRI}$, which is computed by linear regression on a small sample of patients in which borderline patients are few, while those with mPAP values around 30 mmHg abound.

PA pressure waveforms closely follow the shape of the RHC pressure waveforms. An exact match of the MRI derived sPAP, dPAP and mPAP with the RHC pressures averaged over several cardiac cycles can be achieved by use of a free breathing pulse sequence for the measurement of flow and arterial cross-section. The greater beat-to-beat variation of the RHC waveform, as seen in Figure 3, is due to the real-time pressure variations during the cardiac cycle. The poor interobsever reproducibility of sPAP and dPAP is explained by the poor interobsever reproducibility of the compliance measurement, which is used in the convolution relationship to obtain the pressure waveform.

A recent study used the equilibrium condition at the vessel wall to relate the MPA radius change measured by MRI to the change in MPA pressure during the cardiac cycle [27]. Like in our study, the correlations of pressures calculated from radius change with pressures measured by RHC were modest for mPAP and sPAP, with improved correlation for dPAP [27]. Vessel cross-section radius or area is expected to be an imperfect surrogate for pressure, because the PA area can increase independently of pressure [25].

Two-element versus three-element windkessel

The two-element windkessel model is often compared to the three-element windkessel model, which takes into account the characteristic impedance of the pulmonary artery, in order to evaluate the accuracy of pressure computation with each model. Previous work in animals [16] and humans compared the two models for the purpose of computing pulmonary compliance values from known RHC pressure and MRI flow, and found that the three-element windkessel model overestimates the value of compliance. While implementation of the two-element model is sufficient for proof of principle, we believed it was important to do our own comparison with the three-element windkessel model, to account for blood impedance and to better characterize load on the right ventricle. As shown in the results section, the use of the three-element windkessel had no effect. Lungu et al., by fitting a three-element Windkessel model with no assumption of reflectionless and unidirectional pressure waves to pressure and flow data, found that distal vascular resistance increases and compliance decreases significantly with PH severity, while characteristic impedance shows no significant changes [27]. These findings show that improved quantification of the pressure waveforms, and characterization of PH severity, relies on accurate measurement of volume compliance C and PVR, as well as mPAP by MRI. Calculation of mPAP and PVR at MRI through linear regression of RHC mPAP and MRI volume parameters in a larger cohort of patients with similar degree of PH will improve the accuracy of our pressure quantification.

In addition to lump models like the windkessel, impedance spectra and transmission line models have been used for characterizing PH. Impedance models describe vascular opposition to pulsatile flow as a spectrum (magnitude and phase) dependent on frequency. At zero frequency, the vascular impedance magnitude corresponds to PVR, whereas at high frequencies, it corresponds to the ratio of inertial to compliance effects in the large arteries. High fidelity flow and pressure time waveforms must be measured and sampled to compute the impedance spectrum, which does not allow non-invasive measurement of pressure. Moreover, the impedance spectrum describes the disease state by graphical display as a function of frequency, rather than a number or set of numbers, like mPAP, PVR and C, which may make it less useful in the clinical setting.

Non-invasive characterization of PH

MRI measurement of the PA pressures can be used as a non-invasive screening tool for patients suspected of PH. Typically, PH patients present for RHC evaluation with symptoms of dyspnea and echocardiogram evidence of elevated right ventricular systolic pressures (RVSP). Echocardiography is widely accepted as an effective screening tool for PH because it is fast, non-invasive, easy to obtain and provides useful information on cardiac function. RVSP, which is a surrogate for pulmonary artery systolic pressure (PASP), is estimated with echo by measuring the velocity of the tricuspid regurgitant jet [30]. Alternatively, mPAP can be estimated using the PA acceleration time, the peak pulmonic regurgitation gradient, or by tracing the continuous wave Doppler tricuspid regurgitation profile and calculating the mean pressure gradient. Doppler assessment of mitral inflow, mitral annular tissue velocities, and pulmonary venous waveforms combined with left atrial volumes at echocardiography is useful in distinguishing PAH from PVH [31]. However, there is evidence that both mPAP

and PASP as measured by echocardiography may be unreliable due to poor visualization of tricuspid and pulmonary valve insufficiency [32,33]. A study utilizing echocardiography to screen scleroderma patients found 25% of those with PAH on screening echocardiogram to have normal hemodynamic findings at RHC [34]. Moreover, a study comparing SV and PASP measured by echocardiography, phase contrast MRI and RHC found greater agreement between MRI and RHC than between echocardiography and RHC [35]. These findings suggest that MRI has potential to replace echocardiography as a pre-RHC screening tool in patients with suspected PAH.

We followed the methodology of prior authors, who assumed pressure and flow waves to be unidirectional and reflectionless along short portions of the proximal pulmonary arteries. Quick et al have shown that this assumption is as good a description of the arterial system as impedance spectra accounting for reflections in elderly patients with stiffer arteries [19,20]. However, Laskey et al.[14] and others [27,36], challenged this assumption in their study of the pulmonary impedance spectrum in PAH patients at rest and during exercise, by showing that the pulmonary pressure wave can be decomposed into forward and reflective waves. The reflection coefficients measured in healthy volunteers and experimental animals are small [37], but increase at rest [27] and at exercise in PH patients [14], or under acute PH induced in animal models [38]. While the study of the forward and reflective pressure waves may be a worthwhile exercise, it is the sum of these waves that is measured by standard RHC and used for diagnosis. This paper presents an MRI method by which the pressure wave and mPAP are measured non-invasively, with the goal to improve the non-invasive assessment of patients with PH. Thus, measurement of pressure wave reflection components, an interesting topic of future study, is beyond the scope of this paper.

Despite our assumption of reflectionless pressure and flow waveforms, we obtained good agreement between our model and RHC for sPAP and dPAP, when using the MRI flow waveform and the RHC parameters in the calculation of the pulmonary arterial pressure waveform P(t). This proves the two element windkessel model is sufficient for the calculation of pressure from flow, provided an accurate measurement of the input parameters.

Limitations

There were a number of limitations to this study. The current study was meant as proof of concept, so the sample size is small. The small sample size precluded separation of patients into a derivation and a validation cohort. Furthermore, echocardiograms were performed further apart in time from the RHC exam than the MRI exam; ideally, all three tests should have been performed on the same day. Due to the time elapse between the tests, we cannot affirm with certainty if MRI is more effective than echocardiography at measuring the E/e′ ratio.

The temporal resolution of the MRI flow waveforms was limited by a 20 second breath-hold. Shorter acquisition time necessitates lower temporal resolution, compromising resolution of the flow systolic peak and the pressure systolic peak. The accuracy and reproducibility of flow, C, mPAP and PVR measurements will be increased by use of a free-breathing phase contrast sequence with higher temporal resolution and acceleration.

In conclusion, we have obtained proof-of-principle results for an entirely non-invasive MRI based method to assess pulmonary hemodynamic parameters in patients with suspected pulmonary hypertension. Future work involves validation of our method in a larger cohort of patients.

Acknowledgments

Grant Support:

National Institutes of Health, US, grant R01 NS0493395 (Carroll)

National Institutes of Health, US, R01 HL088437 (Carroll)

This work was supported in part by the grant R01 NS049395-04. We thank Jennifer McDonald, RN, for assistance with patient recruiting, Marie Wasielewksi, RT, and Maria Carr, RT, for assistance with scanning patients.

References

1. Gan CT, Lankhaar JW, Westerhof N, Marcus JT, Becker A, Twisk JW, Boonstra A, Postmus PE, Vonk-Noordegraaf A. Noninvasively assessed pulmonary artery stiffness predicts mortality in pulmonary arterial hypertension. Chest. 2007; 132(6):1906–1912. [PubMed: 17989161]
2. Saouti N, Westerhof N, Postmus PE, Vonk-Noordegraaf A. The arterial load in pulmonary hypertension. Eur Respir Rev. 2010; 19(117):197–203. [PubMed: 20956192]
3. Barst RJ, McGoon M, Torbicki A, Sitbon O, Krowka MJ, Olschewski H, Gaine S. Diagnosis and differential assessment of pulmonary arterial hypertension. J Am Coll Cardiol. 2004; 43(12 Suppl S):40S–47S. [PubMed: 15194177]
4. Lam CS, Roger VL, Rodeheffer RJ, Borlaug BA, Enders FT, Redfield MM. Pulmonary hypertension in heart failure with preserved ejection fraction: a community-based study. J Am Coll Cardiol. 2009; 53(13):1119–1126. [PubMed: 19324256]
5. Hoeper MM, Lee SH, Voswinckel R, Palazzini M, Jais X, Marinelli A, Barst RJ, Ghofrani HA, Jing ZC, Opitz C, Seyfarth HJ, Halank M, McLaughlin V, Oudiz RJ, Ewert R, Wilkens H, Kluge S, Bremer HC, Baroke E, Rubin LJ. Complications of right heart catheterization procedures in patients with pulmonary hypertension in experienced centers. J Am Coll Cardiol. 2006; 48(12):2546–2552. [PubMed: 17174196]
6. Nagueh SF, Appleton CP, Gillebert TC, Marino PN, Oh JK, Smiseth OA, Waggoner AD, Flachskampf FA, Pellikka PA, Evangelisa A. Recommendations for the evaluation of left ventricular diastolic function by echocardiography. Eur J Echocardiogr. 2009; 10(19270053):165–193. [PubMed: 19270053]
7. Nagueh SF, Middleton KJ, Kopelen HA, Zoghbi WA, Quinones MA. Doppler tissue imaging: a noninvasive technique for evaluation of left ventricular relaxation and estimation of filling pressures. J Am Coll Cardiol. 1997; 30(6):1527–1533. [PubMed: 9362412]
8. Westerhof N, Lankhaar JW, Westerhof BE. The arterial Windkessel. Med Biol Eng Comput. 2009; 47(2):131–141. [PubMed: 18543011]
9. Vulliemoz S, Stergiopulos N, Meuli R. Estimation of local aortic elastic properties with MRI. Magn Reson Med. 2002; 47(4):649–654. [PubMed: 11948725]
10. Oppenheim, A.; Willsky, A.; Hamid, S. Signals and Systems. Prentice Hall; 1996.
11. Saouti N, Westerhof N, Helderman F, Marcus JT, Stergiopulos N, Westerhof BE, Boonstra A, Postmus PE, Vonk-Noordegraaf A. RC time constant of single lung equals that of both lungs together: a study in chronic thromboembolic pulmonary hypertension. Am J Physiol Heart Circ Physiol. 2009; 297(6):H2154–2160. [PubMed: 19801491]
12. Chesler NC, Roldan A, Vanderpool RR, Naeije R. How to measure pulmonary vascular and right ventricular function. Conf Proc IEEE Eng Med Biol Soc. 2009; 2009:177–180. [PubMed: 19964469]

13. Lankhaar JW, Westerhof N, Faes TJ, Marques KM, Marcus JT, Postmus PE, Vonk-Noordegraaf A. Quantification of right ventricular afterload in patients with and without pulmonary hypertension. Am J Physiol Heart Circ Physiol. 2006; 291(4):H1731–1737. [PubMed: 16699074]
14. Laskey WK, Ferrari VA, Palevsky HI, Kussmaul WG. Pulmonary artery hemodynamics in primary pulmonary hypertension. J Am Coll Cardiol. 1993; 21(2):406–412. [PubMed: 8426005]
15. Muthurangu V, Atkinson D, Sermesant M, Miquel ME, Hegde S, Johnson R, Andriantsimiavona R, Taylor AM, Baker E, Tulloh R, Hill D, Razavi RS. Measurement of total pulmonary arterial compliance using invasive pressure monitoring and MR flow quantification during MR-guided cardiac catheterization. Am J Physiol Heart Circ Physiol. 2005; 289(3):H1301–1306. [PubMed: 15879483]
16. Segers P, Brimioulle S, Stergiopulos N, Westerhof N, Naeije R, Maggiorini M, Verdonck P. Pulmonary arterial compliance in dogs and pigs: the three-element windkessel model revisited. Am J Physiol. 1999; 277(2 Pt 2):H725–731. [PubMed: 10444499]
17. Reuben SR. Compliance of the human pulmonary arterial system in disease. Circ Res. 1971; 29(1): 40–50. [PubMed: 5561407]
18. Gnudi G. New closed-form expressions for the estimation of arterial windkessel compliance. Comput Biol Med. 1998; 28(3):207–223. [PubMed: 9784960]
19. Quick CM, Berger DS, Hettrick DA, Noordergraaf A. True arterial system compliance estimated from apparent arterial compliance. Ann Biomed Eng. 2000; 28(3):291–301. [PubMed: 10784093]
20. Quick CM, Berger DS, Noordergraaf A. Apparent arterial compliance. Am J Physiol. 1998; 274(4 Pt 2):H1393–1403. [PubMed: 9575945]
21. Sanz J, Kariisa M, Dellegrottaglie S, Prat-Gonzalez S, Garcia MJ, Fuster V, Rajagopalan S. Evaluation of pulmonary artery stiffness in pulmonary hypertension with cardiac magnetic resonance. JACC Cardiovasc Imaging. 2009; 2(3):286–295. [PubMed: 19356573]
22. Kuehne T, Yilmaz S, Steendijk P, Moore P, Groenink M, Saaed M, Weber O, Higgins CB, Ewert P, Fleck E, Nagel E, Schulze-Neick I, Lange P. Magnetic resonance imaging analysis of right ventricular pressure-volume loops: in vivo validation and clinical application in patients with pulmonary hypertension. Circulation. 2004; 110(14):2010–2016. [PubMed: 15451801]
23. Guetter C, Thavendiranathan P, Jolly M-P, Lu X, Xue H, Simonetti O. Mitral valve annular velocity measurements derived from cine MRI: validation against Doppler echocardiography. Journal of Cardiovascular Magnetic Resonance. 2012; 14(Suppl 1):W19.
24. Shrout PE, Fleiss JL. Intraclass correlations: uses in assessing rater reliability. Psychol Bull. 1979; 86(2):420–428. [PubMed: 18839484]
25. Boerrigter B, Mauritz GJ, Marcus JT, Helderman F, Postmus PE, Westerhof N, Vonk-Noordegraaf A. Progressive dilatation of the main pulmonary artery is a characteristic of pulmonary arterial hypertension and is not related to changes in pressure. Chest. 2010; 138(6):1395–1401. [PubMed: 20495109]
26. Jeong HJ, Vakil P, Sheehan JJ, Shah SJ, Cuttica M, Carr JC, Carroll TJ, Davarpanah A. Time-resolved magnetic resonance angiography: evaluation of intrapulmonary circulation parameters in pulmonary arterial hypertension. J Magn Reson Imaging. 2011; 33(1):225–231. [PubMed: 21182144]
27. Lungu A, Wild JM, Capener D, Kiely DG, Swift AJ, Hose DR. MRI model-based non-invasive differential diagnosis in pulmonary hypertension. Journal of biomechanics. 2014; 47(12):2941–2947. [PubMed: 25145313]
28. Swift AJ, Rajaram S, Hurdman J, Hill C, Davies C, Sproson TW, Morton AC, Capener D, Elliot C, Condliffe R, Wild JM, Kiely DG. Noninvasive estimation of PA pressure, flow, and resistance with CMR imaging: derivation and prospective validation study from the ASPIRE registry. JACC Cardiovasc Imaging. 2013; 6(10):1036–1047. [PubMed: 23769494]
29. Garcia-Alvarez A, Fernandez-Friera L, Mirelis JG, Sawit S, Nair A, Kallman J, Fuster V, Sanz J. Non-invasive estimation of pulmonary vascular resistance with cardiac magnetic resonance. European heart journal. 2011; 32(19):2438–2445. [PubMed: 21624902]
30. McLure LE, Peacock AJ. Imaging of the heart in pulmonary hypertension. Int J Clin Pract Suppl. 2007; (156):15–26. [PubMed: 17663673]

31. Willens HJ, Chirinos JA, Gomez-Marin O, Fertel DP, Ghany RA, Alfonso CE, Hare JM. Noninvasive differentiation of pulmonary arterial and venous hypertension using conventional and Doppler tissue imaging echocardiography. J Am Soc Echocardiogr. 2008; 21(6):715–719. [PubMed: 18325734]

32. Fisher MR, Forfia PR, Chamera E, Housten-Harris T, Champion HC, Girgis RE, Corretti MC, Hassoun PM. Accuracy of Doppler echocardiography in the hemodynamic assessment of pulmonary hypertension. Am J Respir Crit Care Med. 2009; 179(7):615–621. [PubMed: 19164700]

33. Marsan NA, Westenberg JJ, Tops LF, Ypenburg C, Holman ER, Reiber JH, de Roos A, van der Wall EE, Schalij MJ, Roelandt JR, Bax JJ. Comparison between tissue Doppler imaging and velocity-encoded magnetic resonance imaging for measurement of myocardial velocities, assessment of left ventricular dyssynchrony, and estimation of left ventricular filling pressures in patients with ischemic cardiomyopathy. Am J Cardiol. 2008; 102(10):1366–1372. [PubMed: 18993157]

34. Mukerjee D, St George D, Coleiro B, Knight C, Denton CP, Davar J, Black CM, Coghlan JG. Prevalence and outcome in systemic sclerosis associated pulmonary arterial hypertension: application of a registry approach. Ann Rheum Dis. 2003; 62(11):1088–1093. [PubMed: 14583573]

35. Nogami M, Ohno Y, Koyama H, Kono A, Takenaka D, Kataoka T, Kawai H, Kawamitsu H, Onishi Y, Matsumoto K, Matsumoto S, Sugimura K. Utility of phase contrast MR imaging for assessment of pulmonary flow and pressure estimation in patients with pulmonary hypertension: comparison with right heart catheterization and echocardiography. J Magn Reson Imaging. 2009; 30(5):973–980. [PubMed: 19856412]

36. Nichols, WW.; O'Rourke, MF. McDonald's Blood Flow in Arteries: Theoretical, Experimental and Clinical Principles. New York, NY: Hodder Arnold; 2005.

37. Dwyer N, Yong AC, Kilpatrick D. Variable open-end wave reflection in the pulmonary arteries of anesthetized sheep. J Physiol Sci. 2012; 62(1):21–28. [PubMed: 22102164]

38. Vanderpool RR, Kim AR, Molthen R, Chesler NC. Effects of acute Rho kinase inhibition on chronic hypoxia-induced changes in proximal and distal pulmonary arterial structure and function. J Appl Physiol. 2011; 110(1):188–198. [PubMed: 21088209]

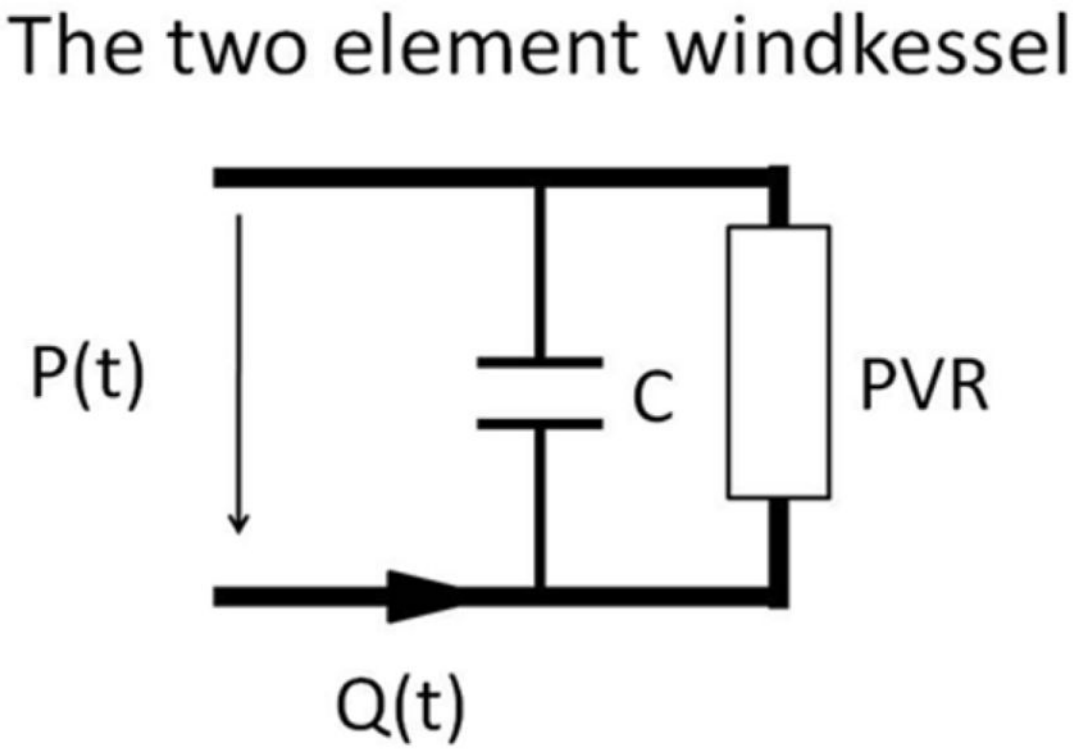

Figure 1.
The two element windkessel model of the pulmonary circulation.

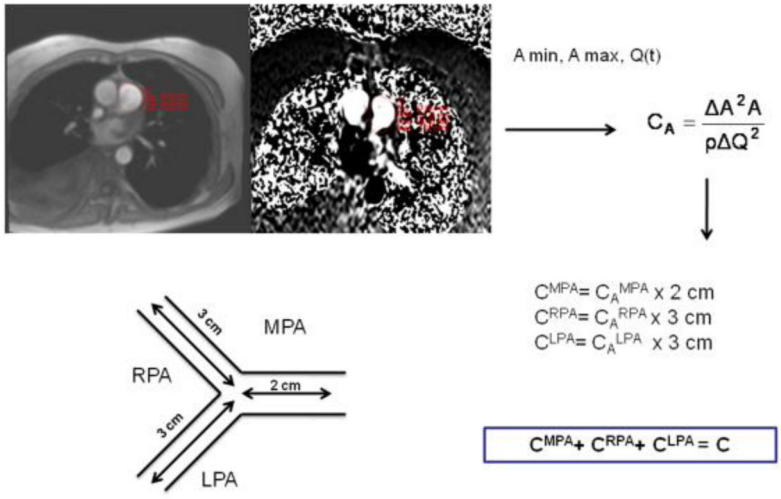

Figure 2.

A schematic diagram describing the measurement of pulmonary arterial compliance by MRI. Total pulmonary arterial compliance is the sum of arterial volume compliances in the main, right and left pulmonary arteries (C^{MPA}, C^{RPA} and C^{LPA}, respectively). These, in turn, are computed from area compliances ($C_A{}^{MPA}$, $C_A{}^{RPA}$ and $C_A{}^{LPA}$), respectively, multiplied by vessels' lengths as reported in the literature.

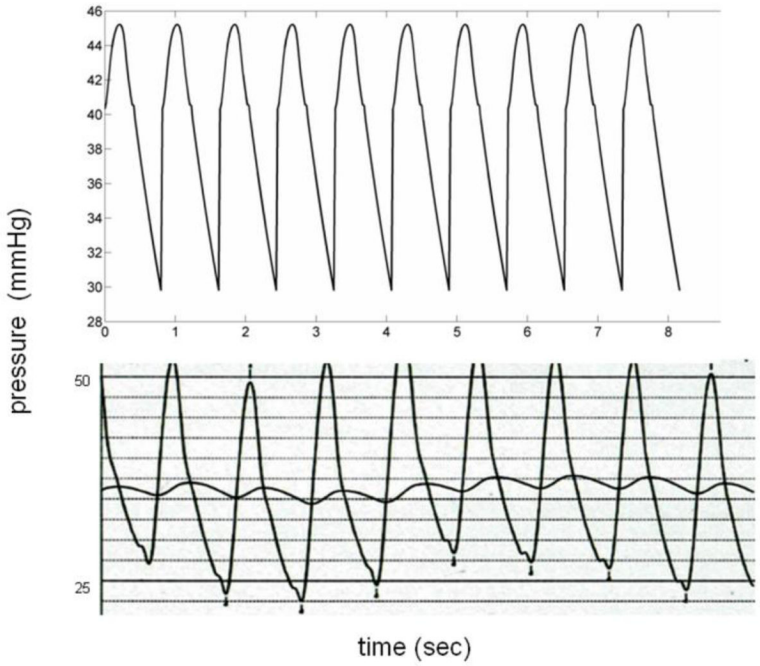

Figure 3.

Comparison of MRI (top) and RHC (down) pressure wave forms in representative patient with PAH (Patient 3). The MRI waveform is free of the variation due to breathing in RHC, and stable, although it results from a flow wave form averaged over 20 seconds.

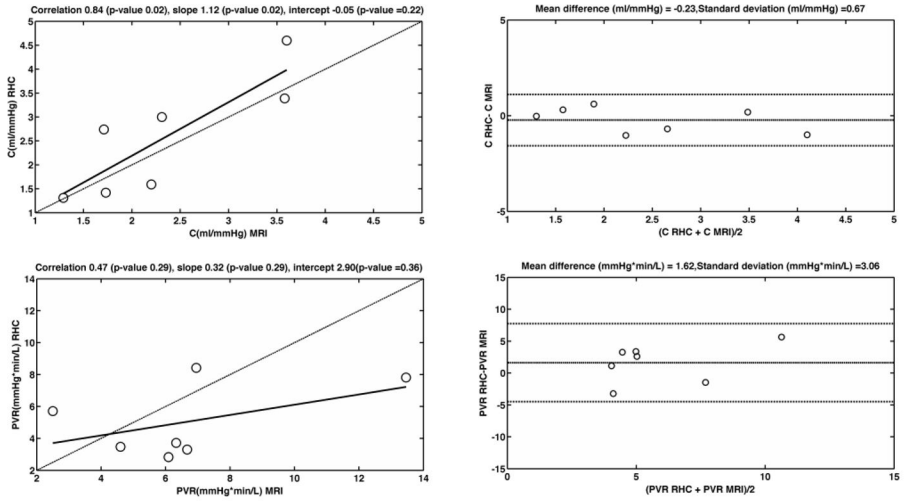

Figure 4.

Bland Altman and correlation plots of C and PVR measured by RHC and MRI. The linearity of the relationship is described by the Pearson correlation. The dashed line on the correlation plots represents the unity line.

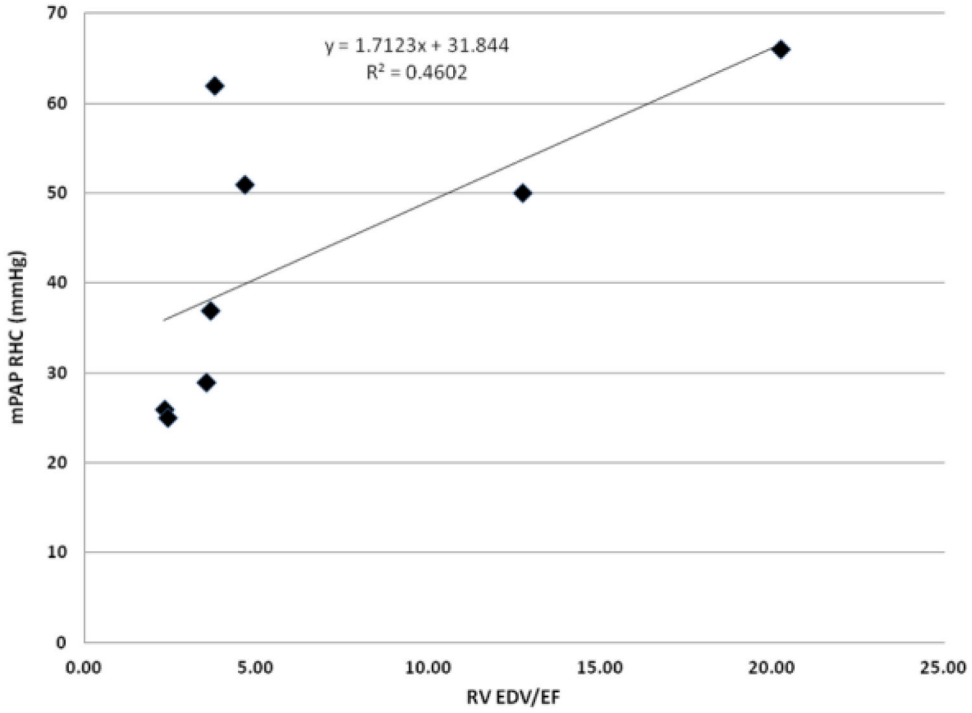

Figure 5.
The linear relationship between RHC mPAP and RV volumetric parameters

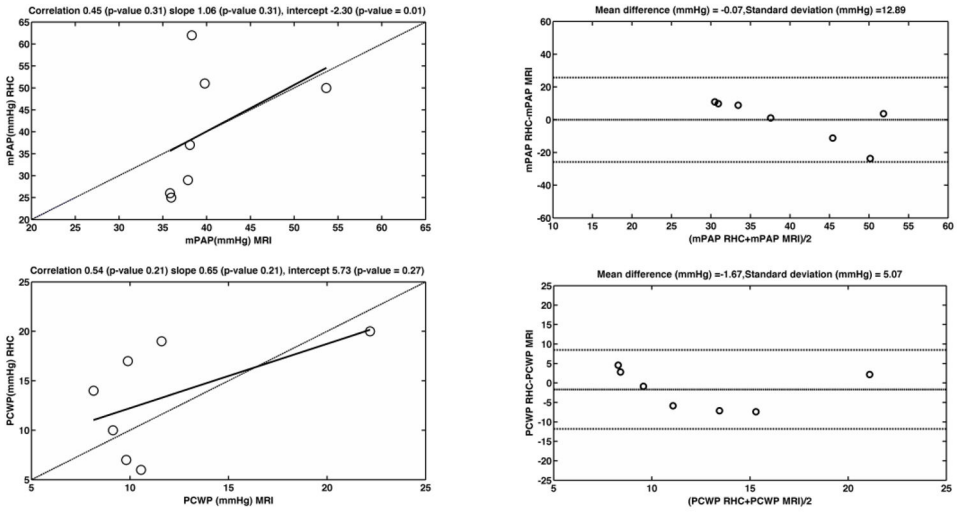

Figure 6.

Bland Altman and correlation plots of mPAP and PCWP measured by RHC and MRI. The linearity of the relationship is described by the Pearson correlation. The dashed line on the correlation plots represents the unity line.

Magn Reson Imaging. Author manuscript; available in PMC 2016 December 01.

Table 1

Summary of measured cardiopulmonary parameters

Parameter	C	C	mPAP	mPAP	PCWP	PCWP	PVR	PVR	dPAP	sPAP	Model dPAP	Model sPAP	Model dPAP	Model sPAP	Model dPAP MRI	Model sPAP MRI
Measurement Method	**RHC**	**MRI**	**RHC**	**MRI**	**RHC**	**MRI**	**RHC**	**MRI**	**RHC**	**RHC**	**MRI**	**MRI**	**RHC**	**RHC**	**RHC**	**RHC**
Patient	**ml/mmHg**	**ml/mmHg**	**mmHg**	**mmHg**	**mmHg**	**mmHg**	**mmHg*min/L**	**mmHg*min/L**	**mmHg**	**mmHg**	**mmHg**	**mmHg**	**mmHg**	**mmHg**	**mmHg**	**mmHg**
1	1.42	1.73	51.00	39.79	20.00	22.18	5.71	2.50	30.00	80.00	17.56	75.96	31.50	79.97	11.56	98.22
2	2.74	1.71	26.00	35.82	7.00	9.81	3.72	6.33	16.00	38.00	25.71	45.87	17.89	33.80	28.91	41.98
3	3.39	3.58	37.00	38.09	17.00	9.89	3.30	6.67	29.00	55.00	31.20	44.98	23.59	52.43	30.73	45.62
4	1.59	2.20	50.00	53.66	14.00	8.15	7.81	13.46	31.00	82.00	45.93	61.08	33.72	68.40	42.97	64.81
5	3.00	2.31	29.00	37.87	6.00	10.56	3.47	4.60	18.00	44.00	27.49	49.71	20.43	39.32	29.21	47.81
6	1.31	1.29	62.00	38.30	19.00	11.60	8.42	6.95	43.00	90.00	19.73	53.26	42.33	84.83	24.34	54.29
7	4.60	3.60	25.00	35.95	10.00	9.14	2.83	6.09	15.00	36.00	24.11	46.69	12.40	38.00	26.36	44.33
Mean	**2.58**	**2.34**	**40.00**	**39.93**	**13.29**	**11.62**	**5.04**	**6.66**	**26.00**	**60.71**	**27.39**	**53.94**	**25.98**	**56.68**	**27.73**	**56.72**
Stdev	**1.22**	**0.92**	**14.47**	**6.21**	**5.71**	**4.78**	**2.30**	**3.37**	**10.20**	**22.81**	**9.37**	**11.20**	**10.36**	**21.07**	**9.31**	**19.86**
p-value		**0.93**		**0.99**		**0.42**		**0.21**			**0.80**	**0.34**	**0.99**	**0.07**	**0.76**	**0.58**
Spearman r		**0.89**		**0.82**		**0.50**		**0.43**			**−0.04**	**0.61**	**1.00**	**0.93**	**−0.04**	**0.79**
ICC intraobserver		**0.78***		**0.97***		**0.99***		**0.83***			**0.81***	**0.90***				
ICC interobserver		**<0.1**		**0.93***		**0.97***		**0.69***			**0.4**	**0.25**				

Compliance (C), mean pulmonary arterial pressure (mPAP), pulmonary vascular resistance (PVR), pulmonary capillary wedge pressure (PCWP), systolic pulmonary arterial pressure (sPAP), diastolic pulmonary arterial pressure (dPAP), measured by right heart catheterization (RHC) and MRI. Intraobserver and interobserver reliability is assessed by the intraclass correlation coefficient (ICC). ICC values significantly different from zero ($p<0.05$) are denoted by *.

Table 2

Compliance measurements with parameters from which compliance was calculated.

Observer 1 Measurement 1																
Patient					**MPA**				**LPA**				**RPA**			
	C	**CMPA**	**CLPA**	**CRPA**	**Amax**	**Amin**	**Qmax**	**Qmin**	**Amax**	**Amin**	**Qmax**	**Qmin**	**Amax**	**Amin**	**Qmax**	**Qmin**
	ml/mmHg	**ml/mmHg**	**ml/mmHg**	**ml/mmHg**	**cm^2**	**cm^2**	**ml/sec**	**ml/sec**	**cm^2**	**cm^2**	**ml/sec**	**ml/sec**	**cm^2**	**cm^2**	**ml/sec**	**ml/sec**
1	1.73	0.30	1.02	0.41	7.74	6.42	312.55	3.59	5.52	4.20	168.64	3.58	5.33	4.61	−166.21	−18.71
2	1.71	0.45	1.02	0.24	5.37	3.06	304.80	3.64	3.35	1.79	137.65	10.85	2.24	1.50	−115.88	−1.20
3	3.58	1.42	1.48	0.68	9.52	6.68	318.55	10.01	3.52	2.04	116.31	9.65	4.36	3.41	−147.24	−15.84
4	2.20	0.15	0.06	1.99	13.47	12.97	251.26	17.48	6.29	6.13	112.92	16.91	5.60	4.48	−106.16	−2.84
5	2.31	0.13	1.65	0.53	9.23	8.37	382.86	36.26	4.68	3.02	152.30	14.32	3.70	2.09	−202.19	−6.62
6	1.29	0.15	0.66	0.48	8.86	8.50	159.47	21.68	6.24	5.86	79.52	9.77	5.73	5.33	−89.66	−7.68
7	3.60	1.65	0.20	1.75	7.98	5.05	255.56	−1.40	1.98	1.52	83.18	4.40	3.99	2.84	−107.73	−17.79
Mean	**2.34**	**0.61**	**0.87**	**0.87**	**8.88**	**7.29**	**283.58**	**13.04**	**4.51**	**3.51**	**121.50**	**9.93**	**4.42**	**3.47**	**−133.58**	**−10.10**
Stdev	**0.92**	**0.65**	**0.60**	**0.70**	**2.45**	**3.13**	**70.24**	**13.09**	**1.63**	**1.92**	**33.57**	**4.83**	**1.25**	**1.41**	**40.04**	**7.26**

Observer 1 Measurement 2																
Patient					**MPA**				**LPA**				**RPA**			
	C	**CMPA**	**CLPA**	**CRPA**	**Amax**	**Amin**	**Qmax**	**Qmin**	**Amax**	**Amin**	**Qmax**	**Qmin**	**Amax**	**Amin**	**Qmax**	**Qmin**
	ml/mmHg	**ml/mmHg**	**ml/mmHg**	**ml/mmHg**	**cm^2**	**cm^2**	**ml/sec**	**ml/sec**	**cm^2**	**cm^2**	**ml/sec**	**ml/sec**	**cm^2**	**cm^2**	**ml/sec**	**ml/sec**
1	1.54	0.07	0.83	0.63	7.79	7.16	314.69	0.03	5.04	4.42	98.90	11.20	5.52	4.56	−171.45	−13.23
2	1.03	0.11	0.58	0.34	5.94	5.00	318.75	3.81	3.90	2.83	159.56	13.87	2.28	1.40	−116.45	−6.68
3	2.68	0.33	1.10	1.24	9.63	8.41	320.61	13.74	3.79	2.63	120.58	10.51	5.01	3.55	−160.23	−8.38
4	2.01	0.32	1.42	0.26	13.29	12.56	248.16	20.17	6.76	5.93	119.72	15.59	5.34	4.97	−100.82	−1.77
5	1.45	0.22	0.94	0.28	8.90	7.62	380.65	4.14	5.02	3.85	159.66	14.34	3.31	2.25	−189.66	−6.52
6	1.34	0.58	0.41	0.35	8.85	8.13	154.77	19.00	6.20	5.90	78.68	8.95	5.83	5.49	−89.97	−7.20
7	2.99	1.25	0.37	1.37	8.20	5.96	244.71	−0.41	2.83	2.08	114.2	5.12	3.47	2.16	−99.95	1.27
Mean	**1.86**	**0.41**	**0.81**	**0.64**	**8.94**	**7.83**	**283.19**	**8.64**	**4.79**	**3.95**	**121.62**	**11.37**	**4.39**	**3.48**	**−132.65**	**−6.07**
Stdev	**0.73**	**0.41**	**0.38**	**0.47**	**2.25**	**2.41**	**73.43**	**8.81**	**1.39**	**1.55**	**29.74**	**3.62**	**1.36**	**1.58**	**40.17**	**4.67**

Magn Reson Imaging. Author manuscript; available in PMC 2016 December 01.

Observer 2
Measurement 1

Patient					MPA				LPA				RPA			
	C	**CMPA**	**CLPA**	**CRPA**	**Amax**	**Amin**	**Qmax**	**Qmin**	**Amax**	**Amin**	**Qmax**	**Qmin**	**Amax**	**Amin**	**Qmax**	**Qmin**
	ml/mmHg	**ml/mmHg**	**ml/mmHg**	**ml/mmHg**	**cm^2**	**cm^2**	**ml/sec**	**ml/sec**	**cm^2**	**cm^2**	**ml/sec**	**ml/sec**	**cm^2**	**cm^2**	**ml/sec**	**ml/sec**
1	1.06	0.03	0.81	0.23	8.11	7.75	302.09	−1.88	4.75	4.15	99.87	17.54	5.74	5.21	−175.11	−18.26
2	1.31	0.08	0.70	0.53	5.58	4.77	314.69	2.06	3.57	2.39	146.99	13.12	2.31	1.24	−106.90	−6.34
3	1.14	0.08	0.49	0.57	9.67	9.10	321.14	14.34	3.91	3.31	113.44	17.58	4.84	3.96	−156.96	−15.22
4	2.39	0.19	0.40	1.80	13.15	12.59	249.66	16.89	6.69	5.68	249.66	16.23	5.26	4.27	−98.24	−3.89
5	0.70	0.10	0.33	0.27	8.81	8.02	365.99	5.39	4.66	4.03	152.11	15.17	3.45	2.48	−191.66	−11.26
6	3.76	0.09	3.26	0.41	8.83	8.55	155.22	19.47	6.28	5.34	82.54	8.38	5.27	4.90	−85.74	−6.94
7	1.19	0.71	0.05	0.44	7.55	5.76	257.01	0.37	2.53	2.29	102.28	5.68	3.25	2.58	−99.15	0.91
Mean	**1.65**	**0.18**	**0.86**	**0.61**	**8.82**	**8.08**	**280.83**	**8.09**	**4.63**	**3.89**	**135.27**	**13.38**	**4.30**	**3.52**	**−130.54**	**−8.72**
Stdev	**1.07**	**0.24**	**1.09**	**0.54**	**2.31**	**2.52**	**68.06**	**8.65**	**1.48**	**1.33**	**56.42**	**4.67**	**1.29**	**1.45**	**42.85**	**6.64**
ICC intraobserver	0.78*	0.57	0.10	0.26	0.99*	0.92*	0.99*	0.38	0.95*	0.94*	0.51	0.73	0.96*	0.97*	0.98*	0.16
ICC interobserver	<0.1	0.33	<0.1	0.66*	0.99*	0.90*	0.99*	0.42*	0.96*	0.89*	0.14	0.27	0.94*	0.96*	0.98*	0.36*

Cross-section maximum area (Amax), minimum area (Amin), maximum flow (Qmax), minimum flow (Qmin) and compliance measurements in the main, left and right pulmonary artery (C MPA, C LPA, C RPA). Intraclass correlation coefficients (ICC) quantify intra-observer and inter-observer agreement for each variable. Statistically significant difference from ICC=0 ($p<0.05$) is denoted by *.

Magn Reson Imaging. Author manuscript; available in PMC 2016 December 01.

Table 3

Right ventricle volume data used to calculate mPAP MRI and PVR MRI.

Patient		Observer 1 Measurement 1				Observer 1 Measurement 2				Observer 2 Measurement 1			
	HR	**RV EF**	**RV EDV**	**RV CO**	**EDV/EF**	**RV EF**	**RV EDV**	**RV CO**	**EDV/EF**	**RV EF**	**RV EDV**	**RV CO**	**EDV/EF**
	bpm	**%**	**ml**	**l/min**		**%**	**ml**	**l/min**		**%**	**ml**	**l/min**	
1	80	43.53	201.9	7.03	4.64	38.77	209.89	6.51	5.41	35.26	195.48	5.51	5.54
2	81	46.73	108.44	4.11	2.32	52.24	112.79	4.77	2.16	51.68	119.07	4.98	2.3
3	74	39.56	144.53	4.23	3.65	45.37	141.4	4.75	3.12	55.63	139.07	5.73	2.5
4	73	19.08	243	3.38	12.74	17.43	280.56	3.57	16.1	20.72	260.93	3.95	12.59
5	85	44.58	156.86	5.94	3.52	44.09	169.61	6.36	3.85	52.16	168	7.45	3.22
6	80	28.93	108.98	3.84	3.77	21.1	155.49	2.62	7.37	21.15	148.21	2.51	7.01
7	52	59.36	142.49	4.4	2.4	45.92	136.98	3.27	2.98	57.55	133.25	3.99	2.32
8	70	16.76	339.33	3.98	20.25	13.97	389.02	3.81	27.85	17.65	370.19	4.58	20.97
ICC intraobserver		0.90*	0.95*	0.86*	0.92*								
ICC interobserver		0.88*	0.97*	0.64*	0.98*								

	Observer 1 Measurement 1				Observer 1 Measurement 2				Observer 2 Measurement 1			
	mPAP MRI	**PVR MRI**	**dPAP MRI**	**sPAP MRI**	**mPAP MRI**	**PVR MRI**	**dPAP MRI**	**sPAP MRI**	**mPAP MRI**	**PVR MRI**	**dPAP MRI**	**sPAP MRI**
	mmHg	**mmHg*min/L**	**mmHg**	**mmHg**	**mmHg**	**mmHg*min/L**	**mmHg**	**mmHg**	**mmHg**	**mmHg*min/L**	**mmHg**	**mmHg**
1	39.79	2.50	17.56	75.96	38.97	2.34	14.55	80.91	40.32	3.13	13.95	85.93
2	35.82	6.33	25.71	45.87	34.61	5.20	17.21	54.92	34.07	4.68	18.60	51.47
3	38.09	6.67	31.20	44.98	35.90	5.37	25.63	46.77	34.45	4.24	11.62	67.24
4	53.66	13.46	45.93	61.08	53.30	12.81	44.61	61.56	53.94	11.49	46.42	60.28
5	37.87	4.60	27.49	49.71	36.87	4.17	20.67	58.14	35.84	3.35	7.34	91.56
6	38.30	6.95	19.73	53.26	41.59	11.95	29.08	50.58	43.16	13.81	38.79	45.98
7	35.95	6.09	24.11	46.69	35.71	8.12	24.62	45.59	34.10	6.20	8.81	66.83
Mean	39.93	6.66	27.39	53.94	39.56	7.14	25.20	56.92	39.41	6.70	20.79	67.04
Standard deviation	6.21	3.37	9.37	11.20	6.50	3.98	9.92	12.07	7.30	4.24	15.50	16.78
ICC intraobserver	**0.97***	**0.83***	**0.81***	**0.90***								

	Observer 1 Measurement 1				Observer 1 Measurement 2				Observer 2 Measurement 1			
	mPAP	**PVR**	**dPAP**	**sPAP**	**mPAP**	**PVR**	**dPAP**	**sPAP**	**mPAP**	**PVR**	**dPAP**	**sPAP**
	MRI	**MRI**	**MRI**	**MRI**	**MRI**	**MRI**	**MRI**	**MRI**	**MRI**	**MRI**	**MRI**	**MRI**
	mmHg	**mmHg*min/L**	**mmHg**	**mmHg**	**mmHg**	**mmHg*min/L**	**mmHg**	**mmHg**	**mmHg**	**mmHg*min/L**	**mmHg**	**mmHg**
ICC interobserver	**0.93***	**0.69***	**0.4**	**0.25**								

Heart rate (HR), right ventricle ejection fraction (RV EF), right ventricle end diastolic volume (RV EDV), right ventricle cardiac output (RV CO), mean pulmonary arterial pressure (mPAP), pulmonary vascular resistance (PVR), diastolic pulmonary arterial pressure (dPAP), systolic pulmonary arterial pressure (sPAP). Intraobserver and interobserver reliability is assessed by the intraclass correlation coefficient (ICC). ICC values significantly different from zero ($p<0.05$) are denoted by *.

Table 4

Left ventricle early diastolic blood velocity E and lateral mitral annulus velocity e′ measurements, from which pulmonary capillary wedge pressure (PCWP) was estimated.

						Observer 1 Measurement 1				Observer 1 Measurement 2				Observer 2 Measurement 1			
Patient																	
	PCWP	**PCWP**	**E**	**e′ lateral**	**E/e′**	**E**	**e′ lateral**	**E/e′**	**PCWP**	**E**	**e′ lateral**	**E/e′**	**PCWP**	**E**	**e′ lateral**	**E/e′**	**PCWP**
	RHC	**echo**	**echo**	**Echo**	**echo**	**MRI**	**MRI**	**MRI**	**MRI**	**MRI**	**MRI**	**MRI**	**MRI**	**MRI**	**MRI**	**MRI**	**MRI**
	mmHg	**mmHg**	**cm/s**	**cm/s**		**cm/s**	**cm/s**		**mmHg**	**cm/s**	**cm/s**		**mmHg**	**cm/s**	**cm/s**		**mmHg**
1	20	15.68	100	9	11.1	90.82	3.6	25.23	22.18	90.82	3.34	27.2	23.72	90.82	3.56	25.5	23.09
2	7	10.77	102.2	14.3	7.15	73.71	7.5	9.83	9.81	74	7.5	9.87	9.82	73.4	6.9	10.6	10.74
3	17	12.01	92.9	11.4	8.15	52.65	5.3	9.93	9.89	52.81	5	10.6	10.37	52.81	5.3	9.96	10.17
4	14	7.64	37	8	4.63	48.2	6.2	7.77	8.15	48.83	6.9	7.08	7.58	48.83	6.1	8	8.54
5	6	9.09	76.5	13.2	5.8	66.8	6.2	10.77	10.56	64.21	6.1	10.5	10.35	65.94	6.1	10.8	10.88
6	19	9.87	45	7	6.43	38.6	3.2	12.06	11.6	37.66	3.6	10.5	10.29	37.36	4.7	7.95	8.5
7	10	16.17	72.5	6.3	11.5	44.06	4.9	9	9.14	42.45	4.7	9.03	9.15	44.06	4.9	8.99	9.37
Mean	**13.29**	**11.6**	**75.16**	**9.89**	**7.83**	**59.26**	**5.27**	**12.08**	**11.62**	**58.68**	**5.31**	**12.1**	**11.61**	**59.03**	**5.37**	**11.7**	**11.61**
Standard deviation	**5.71**	**3.25**	**25.94**	**3.12**	**2.62**	**18.64**	**1.52**	**5.95**	**4.78**	**18.86**	**1.59**	**6.77**	**5.43**	**18.71**	**1.11**	**6.2**	**5.15**
t-test p-value		0.480				0.052	**0.002**	0.069	0.418	0.047	**0.003**	0.094	0.453	0.050	**0.040**	0.1	0.487
Spearman correlation		**0.286**				**0.821**	**0.703**	**0.179**	**0.500**								
ICC intraobserver						**0.9978***	**0.9747***	**0.9871***	**0.9872***								
ICC interobserver						**0.9994***	**0.8924***	**0.9657***	**0.966***								

Velocity measurements by MRI are compared to echocardiography. Pulmonary capillary wedge pressure (PCWP) from MRI is compared to echocardiography (echo) and RHC measurements. Intraobserver and interobserver reliability of the MRI measurements is assessed by the intraclass correlation coefficient (ICC). ICC values significantly different from zero ($p<0.05$) are denoted by *.